TECHNISCHE MECHANIK, 33, 1, (2013), 67 – 84
submitted: July 20, 2012

Combined Shape and Parameter Identification Applied to a Porous Media Simulation

H. Wulf, D. Schellenberg, R. Kreißig, J. Ihlemann

For material parameter estimation as well as shape identification a variety of research and commercial software exists. These tools are often integrated directly into an FEM program or use the FEM solver as a subroutine. However, the two problems are always considered as separate tasks which are solved by separate software packages. When simulating structured specimens, the considered domain often consists of different material types. These are modeled using different material domains. Frequently, the material parameters and the shape of the material domains are unknown. As both components considerably influence the simulation results, separate identification yields poor results. The inhouse identification and optimization software SPC-Opt developed at the department of Solid Mechanics at Chemnitz University of Technology is capable of solving shape and parameter identification simultaneously. Here, the key concept is an abstract formulation of parameters as variables that influence FEM computations. In this paper, the general design and algorithms are presented. Moreover, the application is demonstrated on an academic example using a simple porous media constitutive model.

1 Introduction

For the characterization of materials, the parameters of the material law must be identified from experiments. The standard method consists of applying force and deformation to some carefully designed test specimens. The shape of the specimen and the boundary conditions are usually chosen in such a way that homogeneous deformations can be assumed in a certain area. Therein, measurements are taken, which deliver direct information on the stress-strain relationship. Model parameters are identified by a mean squared error minimization (Luenberger, 1997). Various programs offer the required functionality, for instance the commercial FEM program MSC.MARC.

A decisive drawback of this approach is that the measurement might not contain sufficient information to identify all parameters. Using displacement or stress field information from inhomogeneous experiments increases the information content of the measurements significantly. Then, the Finite Element Method (FEM) is applied to simulate the experiment using the same geometry and boundary conditions. The difference between displacement and stress values computed by FEM and measured data yields the mean squared error. As each optimization process computes the objective function for several parameter sets, several calls to the FEM solver are required. In other words, the FEM can be considered as a subroutine of the optimization.

This method, called inverse FEM, has been applied succesfully to a variety of material parameter identification problems (Mahnken and Stein, 1996; Schnur and Zabaras, 1992; Moritz, 1993). Within several research projects at the Chemnitz University of Technology many material identification problems have been considered by Kreißig et al. (2007), Schellenberg et al. (2007) and Lindner (2010). Parameter identification for porous media was performed by Mahnken and Steinmann (2001), Suh and Olberding (2006) and Hu et al. (2010), for instance.

An essential requirement for inverse FEM is that the geometry of the test specimen and the boundary conditions must be known in order to allow for correct modelling. In addition, material parameters are assumed to be constant over the whole volume of the specimen. These conditions are easy to meet when the test specimens are specifically manufactured for the experiments. However, in some cases structured specimen are more realistic or unavoidable. For instance when investigating biological tissues, the material parameters often depend on the location within the specimen. In addition, the shape can not be chosen arbitrarily. This is especially problematic when dealing with living tissue that must not be removed from the living body. Another application arises if the production process of a material yields a inhomogenous, graded material. For example, it is known that the plastic flow of the material during Cyclic Extrusion Compression (CEC), Cyclic Expansion Extrusion (CEC) and Spin Extrusion is heterogeneous (Richert, 2006; Pardis et al., 2011, 2010). This leads to an inhomogeneous distribution of the material properies withing the processed billet. These findings are supported by microhardness tests. In this paper, a porous media constitutive model is chosen because it is appropriate for many biological tissues and therefore represents a realistic application.

For experiments on living tissue, the test specimen is effectively a small subarea of the whole body. If the area affected by the experiment is small enough, the model can be restricted to the tissue actually investigated. Examples are in-vivo identifications on human liver by Nava et al. (2008) or human brain by Schiavone et al. (2009) made accessible during surgery intervention. When restricting to non-invasive methods, the modelled area must be chosen larger to reproduce the effects to be investigated. Therefore, the model often consists of several material types with different properties or incorporates a continous spatial change of the material parameters.

In consequence, a description of the material parameter distribution is required. The approach employed by Kroon (2010) and Arnold et al. (2011) for instance, consists of identifying a distinct material parameter set per element. In addition, a mesh adaption and refinement algorithm is used by Bangert and Joshi (2008) to pursue an even more flexible strategy: The parameter distribution is discretized by a second FE mesh which may differ from the primary mesh. Both meshes are subject to an adaptive refinement process. Each of these strategies yields large parameter spaces and severely ill-posed inverse problems. Therefore, a Tikhonov type regularization is incorporated by Arnold et al. and Bangerth and Joshi. In Kroon (2010) an iterative subdivision of the material domains in order to obtain a stable identification process is used. Apparently, these approaches offer a great flexibility but require a significant effort in stabilization and a large amount of measured data for a successful identification.

In the present paper, the distribution of material parameters is approximated by a small number material domains with one material parameter set per domain. The shape of the material domains is subject to identification. Hence, a priori knowledge about the general topology of regions of (almost) equal material behavior is required. The space of possible parameter distributions is much smaller in comparison with the aforementioned techniques. In return, a successful identification without additional regularization and on the basis of little input data can be achieved. As a second advantage, the method described in this work does not require any modification of the underlying FE code. Therefore, the full capabilities of commercial FE software is accessible. An example application is the research by Hendriks et al. (2007) on the mechanical properties of skin. They used suction experiments to identify the material parameters for a Mooney-type material law. In addition to the skin layer, the subcoutaneous fat layer was included in the FE model. For each layer, a separate parameter set was identified.

In the case of the research by Hendriks et al. (2007), the thickness of the skin and fat layer was determined by ultrasound images. Obviously, image processing methods are an excellent technique for gathering information on the internal structure of the specimen. However, they require additional measurements and measuring technology. Moreover, the images might not always reveal which areas share the same mechanical properties and should be modelled with a common material domain. Especially when the different material domains are used to approximate a continous change of the material parameters, determining an appropriate shape of the material domains is a challenging task.

Instead of using image generating measurements, it is also possible to determine the geometry from mechanical experiments. The identification of internal shape properties of the specimen can be considered as an optimization problem as well: The shape of the material domains should be optimized with the objective to minimize the mean squared difference between simulation results and measured data. The optimization problem arising is structurally equivalent to shape optimization. The only difference is the interpretation of the obtained shape: Whereas classical shape optimization seeks to find an optimal geometry for parts to be manufactured, here, already existing but unknown geometry properties are sought.

For solving such shape identification problems, the material domains are seperated from each other in the FE model by specific interfaces. They can be approximated by curves and surfaces. As the problems described in the present paper are axially symmetrical, curves are sufficient. Because of the good properties related to shape identification problems, NURBS (Non-rational uniform B-splines) are used for the approximation. Therefore, the topology of the FE mesh depends on the geometry of the interface and has to be readjusted during the variation of the describing NURBS. Consequently, the coordinates of the de Boor points, which are the control points of the NURBS curves, represent the design variables of the shape identification problem.

The drawback of mechanical experiments for shape identification in comparison to image processing techniques is that the optimization process normally requires the knowledge of the correct material parameters. For the identification of material parameters, however, a correct model of the specimen including the shape of the material domains is neccessary. Due to this interdependence, both optimization problems must be solved simultaneously. The central scope of this paper is to demonstrate that this combined optimization is capable of identifying both shape and material parameters from noisy force and displacement measurements.

In order to achieve this goal, first, the similarities of shape and parameter identification are pointed out in Section 2.1. Furthermore, the common implementation into the software package SPC-Opt is presented. For the shape identification part, the parametrization of the interfaces via NURBS and the generation of updated FE meshes is briefly explained. A simple bi-phasic porous media model is chosen as a material law. The essential constitutive equations are summarized in Section 2.3 and the relevant material parameters are indicated.

In Section 2.3, the application of the introduced algorithms to a simple example problem is demonstrated. Due to the academic nature of the example and the basic research characteristic of the issue, no real measurements are available. Instead, synthetic measurements are created by FE simulations with some noise being applied to the results. Nevertheless, the specimen design, the boundary conditions and the input data are chosen with the objective of keeping the experiments simple and realistic. As a preliminary examination, a pure material parameter and a pure shape identification are carried out. Exact information on the corresponding shape or material parameters, respectively, are provided to the optimizer. Finally, the combined identification of shape and material properties is presented.

2 Combined Identification Strategies

2.1 Optimization and Identification with SPC-Opt

The program SPC-Opt (Scientific Parallel Computing and Optimization) has been developed within several research projects at Chemnitz University of Technology. It can be used for shape optimization problems in mechanical engineering as geometry optimization of forming tools (Schellenberg et al., 2010). Furthermore, material parameter identification problems can be solved.

Both shape identification problems as well as material identification problems are second order inverse problems (Moritz, 1993). In most cases, the design variables and material parameters can only be indirectly analyzed by their effect on certain experiments. Typically, a target function Φ adequate to the task is formulated. For shape and material identification problems, the method of least squares is suitable to determine parameters $\boldsymbol{p} = (p_1, ..., p_n)^T$ of constitutive equations. Therefore, the residua are calculated at specific locations $\boldsymbol{r}_i$ and certain instants of time t_i. The value of each residuum R_i is then given by the difference between measured (or artificially generated) data $\bar{y}_i = \bar{y}(t_i)$ of the specimen and predictions of the respective model $\bar{m}(\boldsymbol{p}, \boldsymbol{r}_i, t_i) = y_i(\boldsymbol{p})$ (Nocedal and Wright, 1999)

$$R_i(\boldsymbol{p}) \;=\; \bar{y}_i - \bar{m}(\boldsymbol{p}, \boldsymbol{r}_i, t_i) \;=\; \bar{y}_i - y_i(\boldsymbol{p}) \quad \text{with} \quad i \;=\; 1, ..., m\,. \tag{1}$$

Now the set of parameters $\boldsymbol{p}^*$ has to be found which minimizes the target function $\Phi(\boldsymbol{p})$

$$\boldsymbol{p}^* \;=\; \operatorname{argmin}(\Phi(\boldsymbol{p}))\,,\; \Phi(\boldsymbol{p}) \;=\; \frac{1}{2}\sum_{i=1}^{m}\left[R_i(\boldsymbol{p})\right]^2\,. \tag{2}$$

It is assumed that the target function $\Phi(\boldsymbol{p})$ is sufficiently smooth to use gradient-based optimization methods. To solve the optimization problem, the Levenberg-Marquardt method (Levenberg, 1944; Marquardt, 1963) is adopted. The required gradients $d\Phi(\boldsymbol{p})/d\boldsymbol{p}$ are obtained by evaluating the derivatives of the target function with respect to the design variables and the material parameters. In our work, this is done numerically by using finite differences (Schnur and Zabaras, 1992). Hence, forward differences are applied in this work. Assuming that $\triangle p_j$ is sufficiently small, the derivative with respect to material parameters is approximated by

$$\frac{\partial \Phi}{\partial p_j} \;=\; \frac{\Phi(p_j \,+\, \triangle p_j) \,-\, \Phi(p_j)}{\triangle p_j} \quad \text{with} \quad j \;=\; 1, ..., n\,. \tag{3}$$

Thus, for each varied parameter a single FE simulation has to be carried out. For an increasing number of parameters this leads to high computational costs. With access to high performance computing resources like networks of independant computers (Hennessy and Patterson, 2003; Parhami, 2005) and the High Performance Cluster “CHiC” a large number of processing elements is available at the Chemnitz University of Technology. In consequence, using parallel computing compensates the disadvantages of the numerical methods (Snir, 1998; Lastovetsky, 2003).

2.2 Shape Parametrization

To solve shape optimization problems with SPC-Opt it is necessary to describe the boundary contours of the structure by mathematical functions with the shape parameters as independent variables (Schumacher, 2005). Typical examples of the mathematical representation of edge contours are cubic splines, B-splines or NURBS (nonuniform rational B-splines), which are represented by the vector $\mathbf{P}$ of design variables (de Boor, 2001; Piegl and Tiller, 1995). Unlike B-splines and NURBS, cubic splines pass through all the given nodes. Therefore, the boundary contours of existing FE meshes can be mathematically described with little effort. The control points which determine the contours on the basis of B-splines and NURBS are termed de Boor points. For the latter there also exists a scalar weight for each de Boor point. The procedure is as follows: during generating the finite element mesh using an FEM program, the boundary contour can be easily approximated by cubic splines or a large number of keypoints. But applying the control points of the cubic splines or the keypoints directly to the optimization would produce a large number of design variables. Therefore, the boundary contour is then described by NURBS. Using NURBS leads to two advantages: On the one hand the number of design variables can be significantly reduced. On the other hand an effect on the variation of design variables affects only a limited range of the curve near the control point depending on the order of the NURBS. Therefore, smaller correlations between the design variables can be achieved.

For the generation of the FE meshes, commercial programs are used (ANSYS, MSC.MARC). In this environment, the user creates the initial FE mesh, the boundary conditions, the coordinate systems, and material properties. Additionally, the required boundary contours are described by straight lines, cubic splines or a group of keypoints. The FE nodes have to be tagged and collected in sets in accordance with the corresponding boundary contours. Afterwards, the data format created by the FEM program is converted into a format suitable for SPC-Opt using a conversion program. In addition, the converter includes an algorithm which allows to convert lines and cubic splines to NURBS without significant loss of accuracy (Schneider, 1993). Throughout this process the coordinates and weights of the associated de Boor points are calculated and the user selects the desired coordinates and weights to be assigned as design variables for the shape optimization with SPC-Opt.

In Figure 1 the detail of an FE mesh is shown. The boundary contour of the inner circular arc is approximated by cubic splines. The associated control points correspond to the corner and center nodes of the element edges. At the common nodes of two edges the continuity prevails. The generated NURBS is characterized by the marked de Boor points.

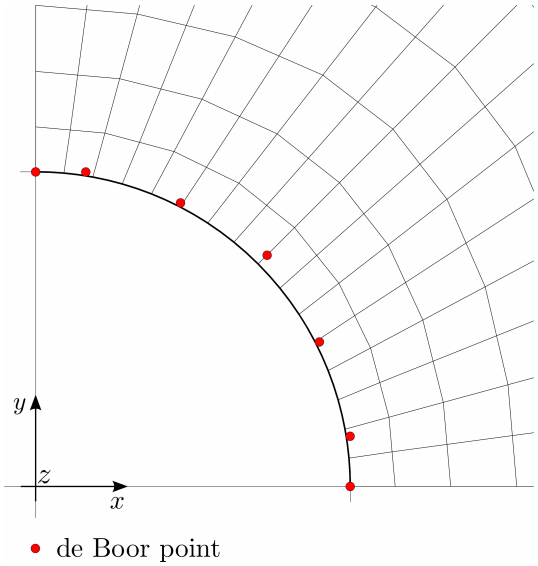

Figure 1: Illustration of a boundary contour with cubic splines and NURBS

If the shape optimization is performed for spatial problems, the described method can equally be applied. In this case, the boundary surfaces are approximated by NURBS surfaces, and the describing de Boor points can be used for optimization in the same way (Elsässer, 1998; Friedrich, 2011).

For solving the direct problems FE meshes have to be generated, that belong to the boundary contour related to the actual values of the design variables and to the contours based on the disturbed design variable sets of the optimization process. In principle, this can be done in two different ways.

One option is to use an automatic mesh generation for every disturbed boundary contour. When using commercial CAD systems, such as Unigraphics and Pro/ENGINEER, the appropriate meshing tools are already available and can be integrated into the optimization process. Usually, the mathematical description of the boundary contours already exists in the corresponding CAD data. Consequently, the shape parameters of the CAD model are directly coupled with the design variables. Thus, after the optimization, the boundary contours of the component in turn are available as CAD data and no conversion is neccessary. The disadvantage of this approach is that in every optimization step for every parameter set a completely new FE mesh is automatically generated and different mesh topologies (changing the number of nodes) can occur. Therefore, this method is not implemented in SPC-Opt.

When using SPC-Opt for solving optimization problems the user creates an FE mesh related to the initial boundary contour. Hence, another way to handle the FE meshes related to the different boundary contours is possible. Thereby, the mesh topology remains unchanged. There is only a variation of the node coordinates performed during the optimization. The quality of the newly generated FE mesh mainly depends on the mathematical algorithm by which the recalculation of the node coordinates is performed. A good method is an appropriate shift of the nodes of the original mesh (Harzheim, 2008). Based on initial coordinates $\boldsymbol{R}^0$, the new node coordinates $\boldsymbol{R}$ can be presented by the shape basis vector $\boldsymbol{T}$ and the design variable p

$$\boldsymbol{R} \;=\; \boldsymbol{R}^0 + p\,\boldsymbol{T}\,. \tag{4}$$

For several design variables prevails

$$\boldsymbol{R} \;=\; \boldsymbol{R}^0 + \sum_{i=1}^{N} p_i\,\boldsymbol{T}_i\,. \tag{5}$$

All design variables are restricted to the subspace which is spanned by the shape basis vectors $\boldsymbol{T}$. The optimal parameters correspond to the minimum of the target function. The determination of $\boldsymbol{T}_i$ must occur such that the solutions of the direct problems are not deteriorated by distortions of the mesh. In the past, virtually no commercial software for the generation of shape basis vectors at an acceptable cost existed. In the meantime, some software packages such as SHAPE200 and MORPHING have become available. Due to the difficulties in calculating the shape base vectors, a different procedure to recalculate the node coordinates is implemented in SPC-Opt and described below.

During the optimization, the coordinates (and weights) of the de Boor points change and so does the boundary contour. As a result, the boundary nodes and inner nodes of the FE mesh have to be shifted accordingly. Therefore, the FE mesh will only be referred to as “nodes” in the following discussion. Their own local coordinate systems (CS) are assigned during the mesh generation process, whereas type and origin can be chosen arbitrarily by the user. Per default the global coordinate system of the FE model is selected. If one or more coordinate directions of a point P are considered to be involved in the shifting process, two reference curves have to be introduced in each direction, so that the point P remains between theese curves. In Figure 2 the combination of lines ($B_{\eta 1}$, $B_{\eta 2}$) and cubic splines ($B_{\xi 1}$, $B_{\xi 2}$) is shown as reference curves in a planar model.

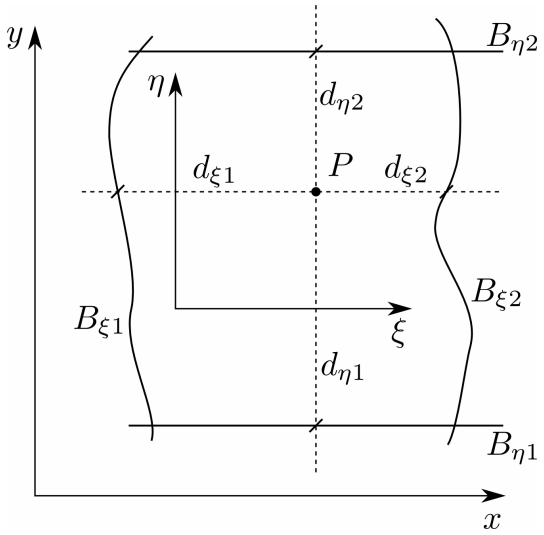

Figure 2: Distance of a node P to the reference curves in cartesian coordinates

The distance between P and the reference curves $d_{\xi 1}$, $d_{\xi 2}$ as well as $d_{\eta 1}$ and $d_{\eta 2}$ lead to the distance ratios

$$\gamma_1 = \frac{d_{\xi 1}}{d_{\xi 1} + d_{\xi 2}} \quad \text{and} \quad \gamma_2 = \frac{d_{\eta 1}}{d_{\eta 1} + d_{\eta 2}}, \tag{6}$$

which are saved for each node. They are used to calculate the new coordinates in accordance with the change of the reference curves. Compliance with the distance ratios (6) is always mandatory. To expand the applications of this approach, local cylindrical coordinate systems can also be used (Figure 3).

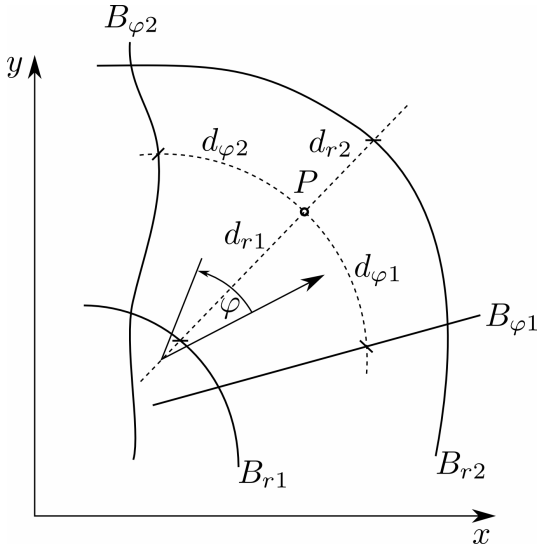

Figure 3: Distance of a node P to the reference curves in cylindrical coordinates

In Figure 4 an FE mesh in the initial state and after the modification of three reference curves is shown. In this example, the local coordinate systems of the nodes correspond to the global cartesian CS.

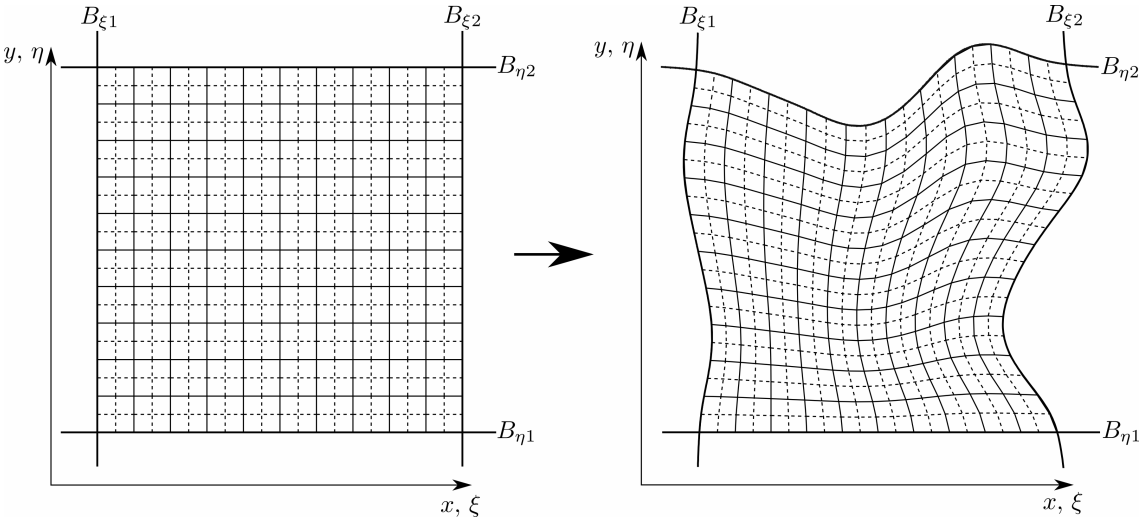

Figure 4: Recalculated FE mesh after distorsion of three reference curves

It is evident that even the distorted mesh has a good quality, whereby the computing time is low. To construct distorted systems with good properties for complex geometries it is necessary to separate the related FE mesh in several areas. It has to be considered that adjacent areas are seperated by the same reference curves which can be defined in different coordinate systems. In case the quality of the FE mesh significantly decreases during the optimization, the problem can optionally be counteracted by using different mesh smoothing algorithms. But this is not necessary for the present example.

2.3 Porous Media Material Model

The presented identification algorithms do not rely on a specific material model. Hence, an arbitrary material behavior can be chosen. As the most realistic application of this combined identification involves research on biological tissues, a material model appropriate for such materials is selected.

Porous media models are often used as material laws for hydrated soft biological tissues (for instance refer to Ehlers and Markert (2001)). The theory of porous media (TPM) assumes that the material consists of a solid and a liquid phase. The liquid is located in the pores of the solid. The pores are assumed to be interconnected and completely filled with pore fluid. According to mixture theory, this structure is replaced by a homogeneous continuum, where each phase is present at each point with a certain fraction. The volume fraction of the liquid is called the porosity Φ_F. Under mechanical loading the pore liquid is forced to flow through the matrix of the solid body. For the pore fluid, incompressible and friction-less behavior is stated. For the solid phase, an arbitrary material law can be chosen, but elastic material behavior is the easiest and most common choice. The only interaction between solid and liquid phase consists of a resistance against the fluid flow induced by the solid matrix.

An excellent introduction to the TPM and its developement is the book by de Boer (2000). Several authors derived constitutive equations, for example Biot (1956), de Boer (2000) and Ehlers and Blum (2002). Especially Ehlers and Blum provide a very general framework including even micropolar or multiphasic materials, for instance. Here, a rather simple material model developed by Görke is used (Görke et al., 2012). The central equations are presented with special attention to the involved material parameters. For a complete description of the material model, the reader is referred to the paper by Görke et al. (2012).

According to Görke, the Cauchy stresses for the solid and fluid phase are

$$\underline{\underline{\sigma}}_S = -\Phi_S \, p \underline{\underline{I}} + \underline{\underline{\sigma}}_S^E \,, \tag{7}$$

$$\underline{\underline{\sigma}}_F = -\Phi_F \, p \underline{\underline{I}} + \underline{\underline{\sigma}}_F^E \,. \tag{8}$$

Here, indices S and F refer to the solid and fluid phase. The volume fraction of the solid phase is $\Phi_S = 1 - \Phi_F$ (complete saturation). Moreover, p denotes the pore pressure, $\underline{\underline{\sigma}}_S^E$ and $\underline{\underline{\sigma}}_F^E$ denote the extra stress of the solid and fluid phase. Assuming ideal fluid behavior, the extra stress of the fluid vanishes. Therefore, the overall stress is

$$\underline{\underline{\sigma}} = -p \underline{\underline{I}} + \underline{\underline{\sigma}}_S^E \,. \tag{9}$$

An equivalent Lagrangian formulation is

$$\underline{\underline{\widetilde{T}}} = \underline{\underline{\widetilde{T}}}_S^E \; - \; p J_S \underline{\underline{C}}_S^{-1} \tag{10}$$

with $\underline{\underline{\widetilde{T}}}$ being the second Piola-Kirchhoff stress tensor, $J_s = \det(\underline{\underline{F}}_S)$ the determinant of the deformation gradient $\underline{\underline{F}}_S$ of the solid phase, and $\underline{\underline{C}}_S = \underline{\underline{F}}_S^T \cdot \underline{\underline{F}}_S$ the right Cauchy-Green Tensor. The second Piola-Kirchhoff extra stress of the solid phase is computed as a derivative of a free Helmholtz energy density Ψ_S

$$\underline{\underline{\widetilde{T}}}_S^E \; = \; 2 \frac{\partial \Psi_S}{\partial \underline{\underline{C}}_S} \,. \tag{11}$$

Görke proposed different functions for the energy density Ψ_S. For the sake of simplicity, the most primitive formulation is chosen

$$\Psi_S \; = \; c_{10}(I_1 - \ln I_3 - 3) + D_2 (\ln I_3)^2 \,. \tag{12}$$

Therein, I_1 and I_3 are invariants of the right Cauchy-Green tensor $\underline{\underline{C}}_S$. The energy function describes a modified neo-Hookean behavior. The material parameters are c_{10} and D_2. They characterize the solid phase and will be subject of the identification.

The contribution of the fluid to the overall stress is governed by the pore pressure. As the pore fluid flow levels out pressure differences, the relation between the pressure gradient and the seepage velocity $\underline{W}_F$ is crucial. Here, a linear relation is assumed (Darcy's law)

$$\underline{W}_F \; = \; -\underline{\underline{K}} \cdot \underline{\nabla}_S \, p \,. \tag{13}$$

The pressure gradient is calculated with respect to the reference configuration of the solid. The permeability tensor $\underline{\underline{K}}$ is a material property, which can be considered as a fluid conductivity. In the paper by Görke et al. (2012), the permeability $\underline{\underline{k}}$ on the current configuration is defined as a material constant. It is related to the Lagrangian permeability tensor $\underline{\underline{K}}$ via the pull-back operation

$$\underline{\underline{K}} = J_S \underline{\underline{F}}_S^{-1} \cdot \underline{\underline{k}} \cdot \underline{\underline{F}}_S^{-T} . \tag{14}$$

In general, the permeability tensor is symmetrica and positive definite. Here, it is assumed to be isotropic, which reduces the number of material parameters to one scalar factor k

$$\underline{\underline{k}} = k \underline{\underline{I}} . \tag{15}$$

To solve the model equations numerically, spatial and time discretization is required. This leads finally to a matrix equation of the form

$$\begin{pmatrix} K & B \\ B^T & -C \end{pmatrix} \begin{pmatrix} \Delta u_s \\ \Delta p \end{pmatrix} = \begin{pmatrix} f \\ g \end{pmatrix} , \tag{16}$$

which represents an FE equation system in two field quantities, the displacement of the solid phase u_s and the pore pressure p. The relations for the components of the stiffness matrix K,B and C as well as the right-hand side f and g are derived in the paper by Görke et al. (2012). The material model and the required solution algorithms for dual-field problems are implemented into the FEM programm SPC-FEM developed at Chemnitz University of technology.

All in all, the presented model is a very simple, almost minimal material law for porous media. It is governed by only three material parameters: the elastic parameters c_{10} and D_2 as well as the permeability k.

3 Application to a Dual-Phase Tissue Cylinder

3.1 Problem Definition

In order to test the algorithms, an academic example has been designed. A simple test specimen and two load cases are defined. The measurements are obtained synthetically from a numerical simulation. In order to receive more realistic measured data, an additive noise is applied. Then, the algorithm is started with the objective to re-identify material and shape parameters.

An advantage of this approach is that the modelling step is easy since boundary conditions and geometry are known. The exact solution is known as well. Therefore, the performance of the algorithm can be easily analyzed. The quality of the input data can be steered via the noise level, allowing to invesigate on the influence of measurement errors. Moreover, the numerical experiment can be done faster and cheaper not involving real measurements. In order to gain valid results concerning the capabilities of the algorithm, the experiment must be kept realistic. Specificially the synthetical measurements should be chosen in such a way that the same values can be measured in a real experiment.

The test specimen, depicted in Figure 5, is an axially symmetric cylinder consisting of two layers with different material behavior. The two layers are placed on top of each other with the lower being material domain one and the upper being material domain two. The thickness of the material layers depends on the distance to the rotation axis. This shape of the interface between the two materials will be the unknown inner shape property to be identified. As material parameters $[k^{(1)}, c_{10}^{(1)}, D_2^{(1)}] = [0.25\text{mm}^4/\,\text{Ns}, 0.05\text{MPa}, 0.00625\text{MPa}]$ for the lower material domain and $[k^{(2)}, c_{10}^{(2)}, D_2^{(2)}] = [0.05\text{mm}^4/\,\text{Ns}, 0.25\text{MPa}, 0.03125\text{MPa}]$ for the upper domain are used. In other words, the lower layer is significantly softer and more permeable than the upper layer.

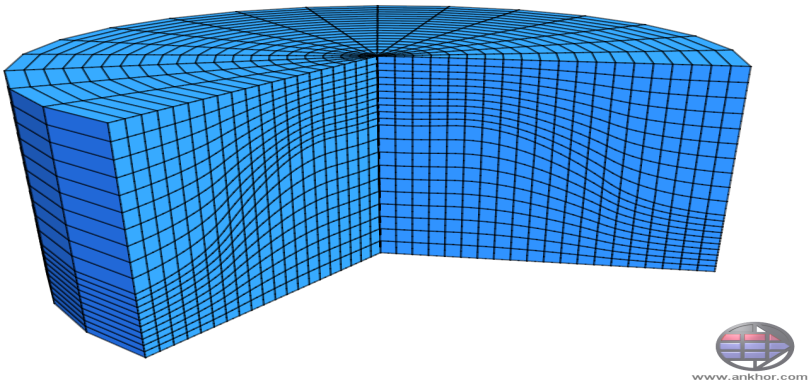

Figure 5: FE model of the test specimen

Two experiments are simulated in order to obtain synthetic measurements. The schematic set-up is depicted in Figures 6 and 7. In general, the lower boundary is completely fixed and does not allow for fluid flow. On the contrary, the pore fluid can flow across the top and the lateral surface, which is achieved by a Dirichlet boundary condition of $p = 0$. On the top surface, a time-dependent displacement $u_z(t)$ is applied using a permeable, cylindrical indenter. For the first experiment, the indenter has the same radius as the cylinder. However, the identification attempts revealed that this experiment is insufficient for collecting enough information. It essentially delivers merely global data and little information on the internal shape of the interface Γ. As a consequence of this, the second experiment with halved indenter radius is devised. Here, the displacement is applied to the inner circle-shaped quarter of the area.

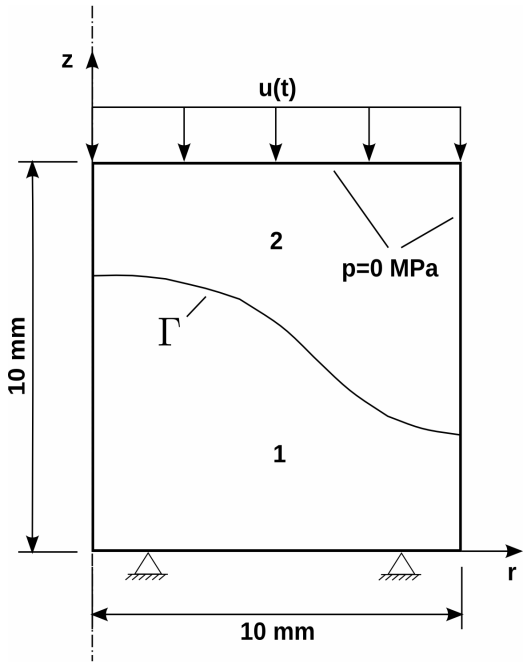

Figure 6: Schematic set-up of Experiment 1

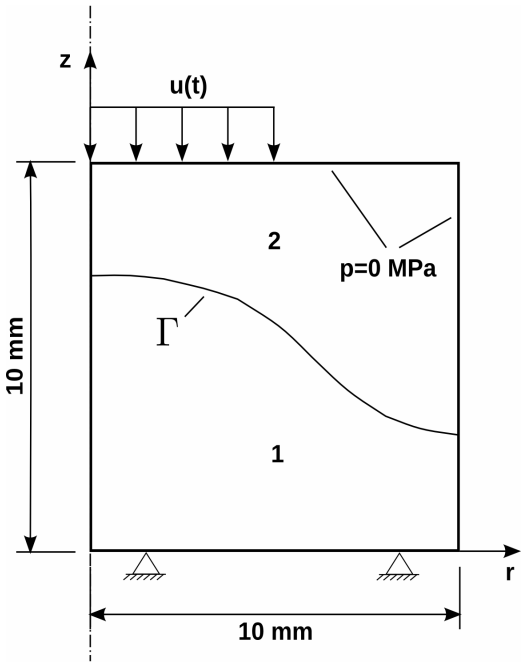

Figure 7: Schematic set-up of Experiment 2

The displacement function $u_z(t)$ shown in Figure 8 is a linear function reaching 15% of the overall height of the cylinder at time $T_1 = 100s$. Afterwards, displacement is kept constant until $T = 400s$.

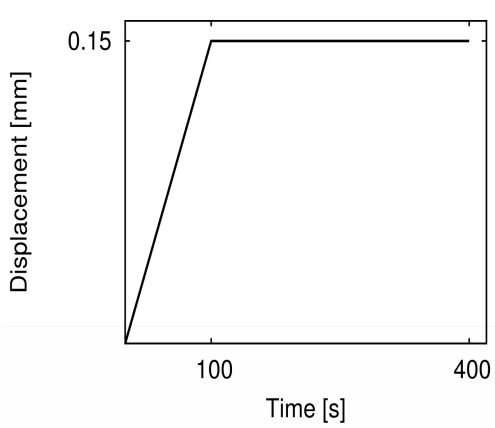

Figure 8: Function of the prescribed displacement of the upper edge

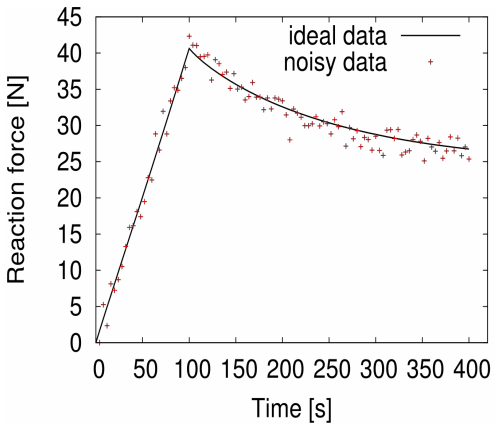

Figure 9: Ideal and noisy reaction force computed for the first experiment

The reaction force at the indenter is used as a synthetic measurement. In addition, the displacement field at the free boundaries is computed. This includes the lateral surface in both cases, but also the part of the top surface not covered by the indenter for the second experiment. No data from the inside of the specimen is incorporated. This restriction is intentional. In the current set-up, the complete displacement fields are easily available. In a real experiment, gathering information from the inside of the specimen requires image processing methods like ultrasound again (Hendriks et al., 2007). In contrast, the proposed measured data can be obtained by a simple force meter and optical methods. The restriction that only information on the boundary is available is essential for defining a realistic challenge for the algorithm.

The reaction force is computed at 100 equidistant instants of times (each 4 seconds). The displacement fields at the free boundary are generated at 20 equidistant instants (each 20 seconds). Gaussian noise is applied to all synthetic measurements in order to gain more realistic data. The standard deviation of the noise is 5% of the maximum pressure and maximum displacement occuring for the respective experiment. As an example, the exact and noisy reaction force for the first experiment are shown in Figure 9.

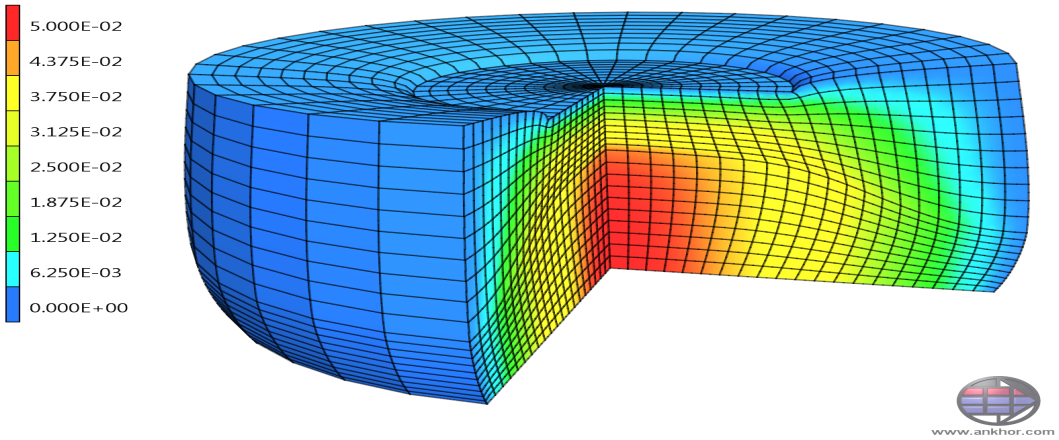

Figure 10: Deformed specimen and pressure field after $t = 100s$ for the second experiment

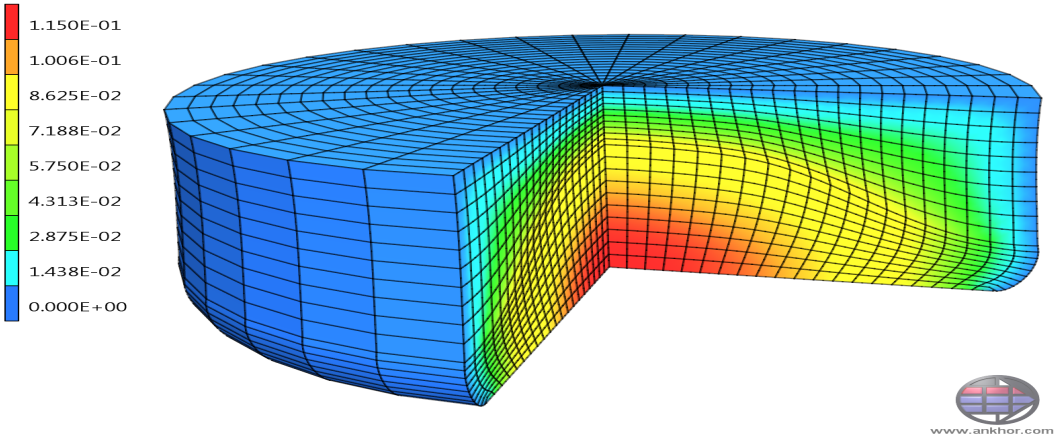

Figure 11: Deformed specimen and pressure field after $t = 100s$ for the first experiment

To illustrate the two experiments, the deformed shapes with the pore pressure distribution are displayed in Figures 10 and 11. Both images are generated at $t = 100s$, which is the time when the largest pore pressure values occur. The large deformations as well as the different material behavior of the two layers can be easily seen. Moreover, the pressure field clearly outlines the interface between the material domains.

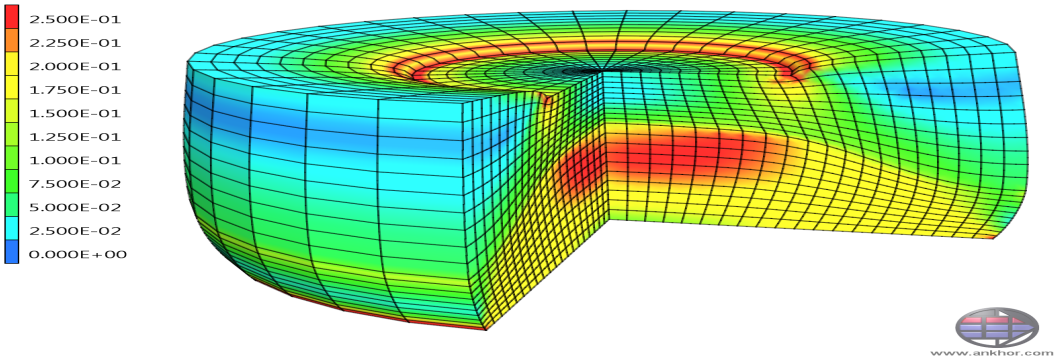

Figure 12: Deformed specimen and von Mises equivalent strain field after $t = 125s$ for the first experiment

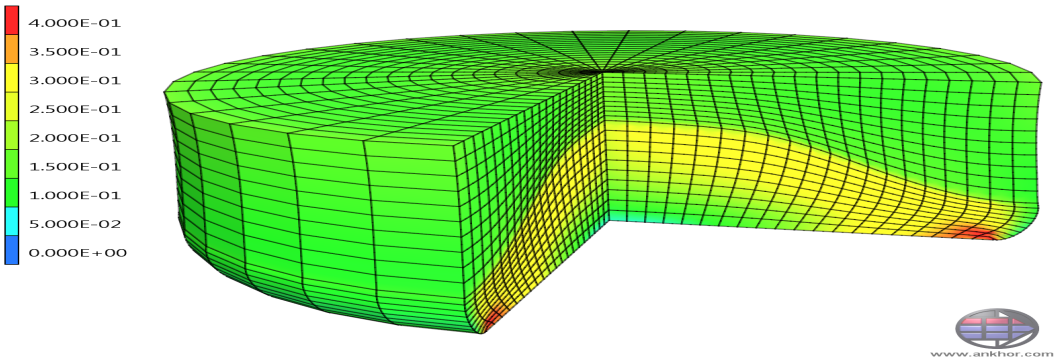

Figure 13: Deformed specimen and von Mises equivalent strain field after $t = 125s$ for the second experiment

The von Mises equivalent strain fields are depicted in Figures 12 and 13. The different material domains are clearly visible. Apparently, an identification of the interface shape would be easy when given the whole strain field. Unfortunately, gathering this information in real cases is almost impossible. Moreover, the inhomogeneous strain field shown in Figure 13 demonstrates, why this experiment is suitable for collecting additional data on the inner volume.

3.2 Material Parameter Identification

As a first preliminary experiment, a re-identification of the material parameters is performed. Specifically, the parameter vector $[k^{(1)}, c_{10}^{(1)}, D_2^{(1)}, k^{(2)}, c_{10}^{(2)}, D_2^{(2)}]$ is identified. The optimizer is supplied with the exact shape of the specimen and the interface. The identification is started with exact measurements first and with noisy input again. The initial parameters are set to $[k = 0.2\text{mm}^4\text{N}^{-1}\text{s}^{-1}, c_{10} = 0.2\text{MPa}, D_2 = 0.02\text{MPa}]$ for both material domains. The identification converges after 8 steps in both cases. The results are presented in Table 1.

Parameter	True value	Initial value	Optimized	Optimized (noise)
$k^{(1)}[\text{mm}^4\text{N}^{-1}\text{s}^{-1}]$	0.25	0.2	0.249	0.235
$c_{10}^{(1)}[\text{MPa}]$	0.05	0.2	0.0499	0.0496
$D_2^{(1)}[\text{MPa}]$	0.00625	0.02	0.00623	0.00598
$k^{(2)}[\text{mm}^4\text{N}^{-1}\text{s}^{-1}]$	0.05	0.2	0.0502	0.0558
$c_{10}^{(2)}[\text{MPa}]$	0.25	0.2	0.00249	0.248
$D_2^{(2)}[\text{MPa}]$	0.03125	0.02	0.0313	0.0316

Table 1: Optimization results of the pure material parameter identification

Using ideal measurements, the material parameters could be re-identified almost perfectly. The remaining error is due to the algorithm tolerance and the numerical differentiation scheme. With the noisy input, deviations up to 11.2% occur. Especially the permeability values are disturbed. These parameters are mainly identified by the relaxation of the reaction force. As rather few force values are present compared to the displacement values, these are more sensitive to noise. When considering the noise level of 5%, this result represents a good re-identification.

3.3 Shape Parameter Identification

In a second experiment, only the shape of the interface is identified. The material parameters are assumed to be known. The interface shape is parametrized with a third-order NURBS using 5 equidistant de Boor points placed at $[r_1 = 0, r_2 = 2.5, r_3 = 5, r_4 = 7.5, r_5 = 10]$mm. Furthermore, the first de Boor point is internally treated as triple point to enforce that the left end of the NURBS is horizontal. This ensures that the axially symmetric interface is a smooth surface without a tip at the center. The z coordinates of the de Boor points are the shape parameters to be optimized. The radial position of the de Boor points is kept constant. As initial parameters, $[z_1, z_2, z_3, z_4, z_5] = [5\text{mm}, 5\text{mm}, 5\text{mm}, 5\text{mm}, 5\text{mm}]$ are chosen. Thus, as initial guess, both layers have a constant thickness of exactly half the height of the model. The corresponding initial model is depicted in Figure 14. Note that this initial shape differs significantly from the desired target shape. No a-priori information is adopted.

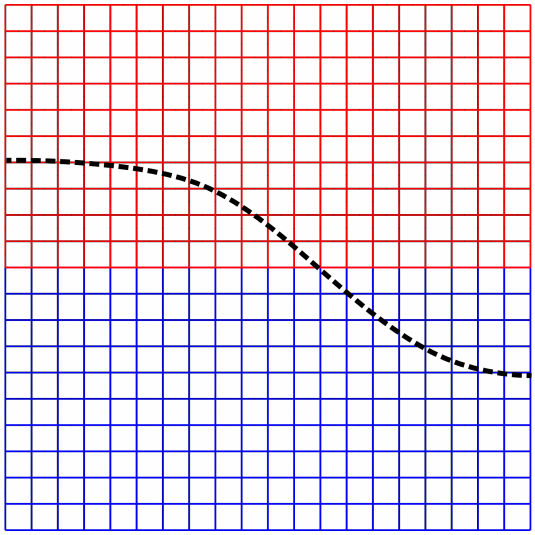

Figure 14: Initial FE model for shape identification. The dashed line represents the correct shape of the interface.

Note that the 5-parameter third-order NURBS is not capable of exactly reproducing the cubic spline which represents the optimal solution. Consequently, perfect re-identification is impossible even with noise-free measurements. In contrast to material parameter identification, no perfect solution can be given. The identification is carried out with ideal and noisy measured data as well. In both cases the optimization converges quickly indicating a well-posed problem structure.

The resulting z coordinates of the de Boor points are presented in Table 2. As de Boor points not neccesarily lie on the NURBS, these values are not very descriptive. Hence, the corresponding adapted FE meshes are displayed in Figures 15 and 16. The identified shape of the interface line can be easily seen there. The cubic spline of the exact interface is added as a dashed line.

Parameter	Initial value	Optimized	Optimized (noise)
$z_1\,[\text{mm}]$	5	7.12	7.16
$z_2\,[\text{mm}]$	5	6.80	6.70
$z_3\,[\text{mm}]$	5	5.74	5.83
$z_4\,[\text{mm}]$	5	3.17	3.19
$z_5\,[\text{mm}]$	5	2.99	2.99

Table 2: Optimization results of the pure shape identification

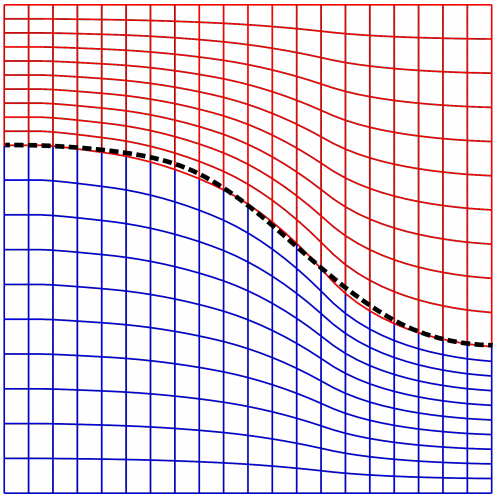

Figure 15: Result of shape identification based on ideal input data. The dashed line represents the correct shape of the interface.

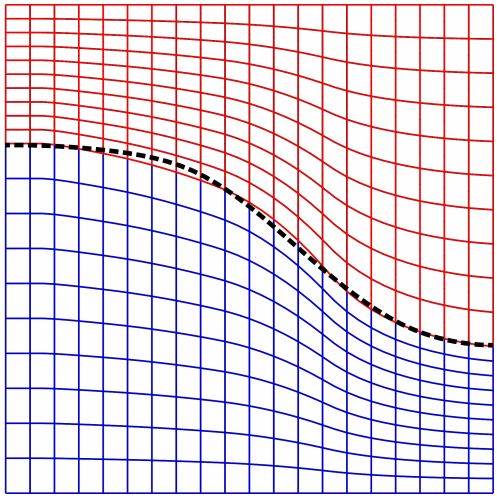

Figure 16: Result of shape identification based on noisy input data.

As expected, the exact shape could not be matched exactly. However, the deviation from the exact solution is small enough to characterize the identication as very succesful. In contrast to the parameter identification, no significant quality difference between perfect and noisy input data could be detected. Apparently, a considerable error is already caused by the imperfect shape discretization. On the other hand, the results can be interpreted such that noise has little impact on the identification.

In general, the largest errors occur at the center of the specimen. This could be expected as well. First, these areas are most remote from the boundaries where measurements are available and where they have little influence on the measured values. Second, interface shape at the center influences a very small part of the overall specimen volume. Alltogether, the sensitivity of the experimental data with respect to the leftmost de Boor point is rather poor.

3.4 Simultaneous Parameter and Shape Identification

In this section, the simultaneous re-identification of shape and material parameters is performed. The shape parametrization is identical to the previous optimization. To be precise, a parameter vector $[z_1, z_2, z_3, z_4, z_5, k^{(1)}, c_{10}^{(1)}, D_2^{(1)}, k^{(2)}, c_{10}^{(2)}, D_2^{(2)}]$ from an eleven-dimensional search space should be found. The initial parameters are set to $[5\text{mm}, 5\text{mm}, 5\text{mm}, 5\text{mm}, 5\text{mm},\ 0.2\text{mm}^4/\,\text{Ns}, 0.2\text{MPa},\ 0.02\text{MPa}, 0.2\text{mm}^4/\,\text{Ns}, 0.2\text{MPa}, 0.02\text{MPa}]$. Hence, the initial shape is the same as shown in Figure 14.

It should be noted that the initial material parameters of both material domains are equal. Hence, the interface shape is irrelevant in the first optimization step. Consequently, the derivatives of the resuduals with respect to the shape parameters are zero and the Hessian matrix is singular. This demonstrates the difficulties arising from the combined identification and the need for stabilized optimization algorithms (Clausner, 2007).

For the combined identification, 12 iteration steps when using ideal input data and 15 steps with noisy input data are required until the algorithm stops. At the beginning of the identification, only the material parameters change significantly. Subsequently, there is a phase with considerable changes in both parameter parts, which also shows the interaction between of the two identification problems. At the end, mainly the shape parameters are shifted to their final value.

The exact values of the identification results are listed in Table 3. The first conclusion is that the identification of the material parameters works as well as the pure material parameter identification. As the relative error values are below 10% for all parameters, the result is very satisfying. Moreover, the noise hardly influences the result quality of the material parameters. Perhaps the main challenge when fitting the material parameters is the unavoidable error in the shape rather than the noisy input. From this viewpoint, it is notable that small deviations of the geometry did not critically disturb the parameter identification.

Parameter	True value	Initial value	Optimized	Optimized (noise)
$k^{(1)}[\mathrm{mm}^4\mathrm{N}^{-1}\mathrm{s}^{-1}]$	0.25	0.2	0.255	0.256
$c_{10}^{(1)}[\mathrm{MPa}]$	0.05	0.2	0.0494	0.0487
$D_2^{(1)}[\mathrm{MPa}]$	0.00625	0.02	0.00608	0.00590
$k^{(2)}[\mathrm{mm}^4\mathrm{N}^{-1}\mathrm{s}^{-1}]$	0.05	0.2	0.04811	0.0479
$c_{10}^{(2)}[\mathrm{MPa}]$	0.25	0.2	0.249	0.247
$D_2^{(2)}[\mathrm{MPa}]$	0.03125	0.02	0.0314	0.0306
$z_1[\mathrm{mm}]$	-	5	6.75	7.02
$z_2[\mathrm{mm}]$	-	5	6.93	6.69
$z_3[\mathrm{mm}]$	-	5	5.59	5.56
$z_4[\mathrm{mm}]$	-	5	3.17	3.16
$z_5[\mathrm{mm}]$	-	5	2.96	2.95

Table 3: Optimization results of the combined material and shape parameter identification

The results of the shape identification are visualized by showing the adapted meshes again (see Figures 17 and 18). First of all, the results are very satisfying, as main properties of the interface shape are succesfully re-identified. Pure shape identification errors mainly occur at the center of the cylinder. Noisy input primarily influences the leftmost two de Boor points. In general, sensitivity of the experimental results with respect to the left-most de Boor points is rather poor. Consequently, small deviations in the input lead to significant differences in the output vector. For future research, either incorporating another experiment or applying some regularisation is advisable (cf. (Shutov and Kreißig, 2010)). Despite these issues, the parameters can be re-identified reliably, although the measurements are noisy. Remarkably, data merely collected on the boundary is sufficient.

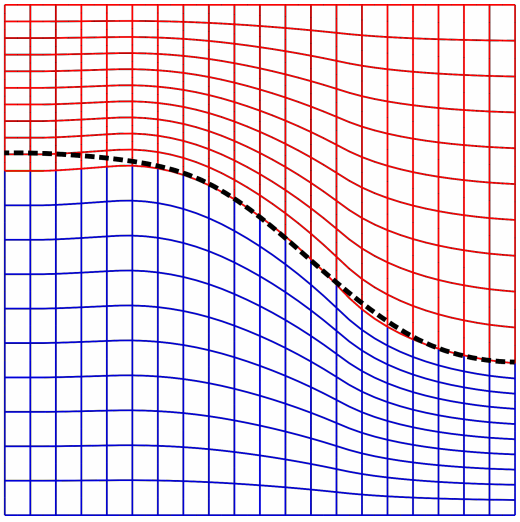

Figure 17: Resulting shape from combined identification based on ideal input data. The dashed line represents the correct shape of the interface.

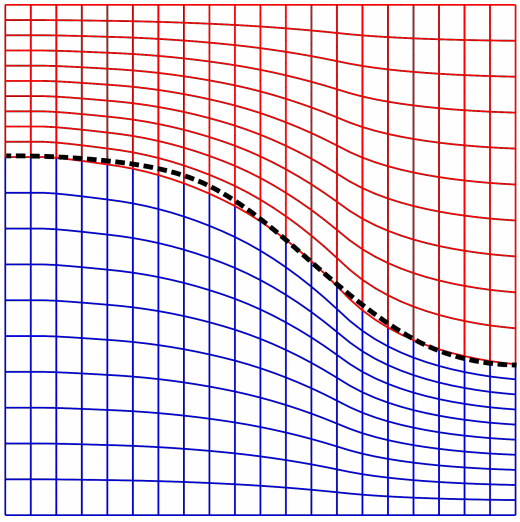

Figure 18: Resulting shape from combined identification based on noisy input data.

Obviously, the presented succesful experiments are the result of an evolutionary process concerning the specimen design and selection of boundary conditions. As a final remark, some of the experiences collected meanwhile shall be shared. First of all, incorporating multiple experiments is almost inevitable. Especially when using only restricted field data, one single experiment never contains a sufficient amount of information. Second, combining global information like reaction forces with field data is very advantageous. Third, the loading speed and relaxation time should be well chosen. According to our experience, the relaxation phase contains most information, if a significant reduction in reaction force occurs at the beginning, but almost equilibrium state is reached at the end. Finally, applying large deformation improves the information content considerably.

4 Conclusion and Outlook

In this paper, an algorithm for simultaneous identification of shape and material identification is presented. To this purpose, an abstract concept of inverse FEM including both shape and parameter identification is developed. For shape identification, the parametrization of curves via NURBS is applied. As material law a simple porous media model is chosen. The presented algorithm for combined identification, however, is applicable for arbitrary material models.

To demonstrate the method, an academic example is designed and solved. The devised test specimen consisted of two material domains with an unknown shape of the interface. The interface is parametrized using NURBS. Two indentation experiments with different indenter sizes are designed to collect the data for identification. The data is obtained as synthetical measurements from numerical simulations with additive Gaussian noise. Moreover, only data available at the boundary of the specimen is used. The aim of this restriction is to ensure that the same data could be easily collected in real experiments.

First, material and shape parameters are identified separately with the respective other parameter set assumed to be known. Both optimzations converged fast returning good results. However, these examinations revealed that the sensitivitiy of the measurements with respect to some parameters is poor. Afterwards, the simultaneous identification of all parameters is executed. The initial parameter vector for identification is chosen far away from the optimum and had identical material parameters for both material domains. Nevertheless, the solution converged quickly and succesfully. Both material and shape properties are closely re-identified with small deviations due to noise. Overall, the example application demonstrates that the algorithm is capable of solving combined shape and parameter identification problems on the basis of realistic input data.

For future research, investigations on practical problems involving real measurements are desirable. As already explained, applications can be found in the field of biomechanics. Specifically, research on mechanical properties and shape of the fat pad on the human heel is planned at Chemnitz University of Technology. However, mixed shape/material parameter identification problems may arise in classical material science as well. An example is nanoindentation, where due to the small size of the indenter manufacturing imperfections become relevant. Although often assumed as perfectly pointy, the tip of the indenter is rounded off with an unknown radius. Identifying this radius alongside with some material parameters might improve the overall quality of the results.

The algorithm itself offers starting points for further research as well. One issue already observed during the work presented in this paper is related to the shape parametrization. Selecting an appropriate number and location of de Boor points is difficult and requires profound experience. Parametrization with too few supporting points overly restricts the space of possible shapes. When the number of de Boor points is chosen to high, the results become very volatile with respect to disturbed input data. While such difficulties are already known for plain shape optimization, a combination with parameter identification provides another additional challenge. Hence, regularization techniques should be considered to stabilize the solution process. In general, further investigations on the properties of this new mixed optimization problem and adapted optimization techniques are desirable.

Bibliography

Arnold, A.; Bruhns, O.; Mosler, J.: An efficient algorithm for the inverse problem in elasticity imaging by means of variational r-adaption. *Phys. Med. Biol.*, 56, (2011), 4239–4265.

Bangert, W.; Joshi, A.: Adaptive finite element methods for the solution of inverse problems in optical tomography. *Inverse Problems*, 24.

Biot, M.: General solution of the equation of elasticity and consolidation for a porous material. *J. Appl. Mech.*, 23, (1956), 91–96.

Clausner, A.: *Anwendung von Line-Search-Strategien zur Formoptimierung und Parameteridentifikation*. Master's thesis, Chemnitz Univerity of Technology (2007).

de Boer, R.: *Theory of porous media: Highlights in Historical Developement and Current State*. Springer Verlag, Berlin (2000).

de Boor, C.: *A practical guide to splines*. Springer Verlag, New York (2001).

Ehlers, W.; Blum, J.: *Porous Media. Theory, Experiments and Numerical Applications*. Springer Verlag, Berlin, Heidelberg (2002).

Ehlers, W.; Markert, B.: Linear viscoelastic biphasic model for soft tissues based on the theory of porous media. *J. Appl. Mech.*, 123, (2001), 418–424.

Elsässer, B.: *Approximation mit rationalen B-Spline Kurven und Flächen*. Diss., RWTH Aachen, Aachen (1998).

Friedrich, L.: *Untersuchung von Flächenapproximationsverfahren mit NURBS-Flächen im Rahmen der 3D-Formoptimierung*. Studienarbeit, Chemnitz Univerity of Technology (2011).

Görke, U.-J.; Kaiser, S.; Bucher, A.; Kreißig, R.: A consistent mixed finite element formulation for hydro-mechanical processes in saturated porous media at large strains based on a generalized material description. *Eur. J. Mech.*, 32, (2012), 88–102.

Harzheim, L.: *Strukturoptimierung, Grundlagen und Anwendungen*. Verlag Harri Deutsch, Frankfurt a.M. (2008).

Hendriks, F.; Brokken, D.; van Eemeren, J.; Oomens, C.; Baaijens, F.; Horsten, J.: A numerical-experimental method to characterize the non-linear mechanical behaviour of human skin. *Skin Research and Technology*, 9, (2007), 274–283.

Hennessy, J.; Patterson, D.: *Computer Architecture: A Quantitative Approach - Third Edition*. Morgan Kaufman Publishers, San Francisco (2003).

Hu, Y.; Zhao, X.; Vlassak, J.; Suo, Z.: Using indentation to characterize the poroelasticity of gels. *Applied Physics Letters*, 96.

Kreißig, R.; Benedix, U.; Görke, U.-J.; Lindner, M.: Identifikation and estimation of constitutive parameters for material laws in elastoplasticity. *GAMM-Mitt.*, 30, (2007), 458–480.

Kroon, M.: An efficient method for material characterisation of hyperelastic anisotropic inhomogeneous membranes based on inverse finite-element analysis and an element partition strategy . *J. Mech. Appl. Math.*, 63, (2010), 201–225.

Lastovetsky, A.: *Parallel Computing on Heterogenous Networks*. Wiley-Interscience, Hoboken New Jersey (2003).

Levenberg, K.: A method in the solution of certain non-linear problems in least squares. *Q. Appl. Math.*, 2, (1944), 164–168.

Lindner, M.: *Ermittlung der plastischen Anisotropie durch Eindringversuche*. Diss., Chemnitz University of Technology, Institut für Mechanik und Thermodynamik (2010).

Luenberger, D.: *Optimization by Vector Space Methods*. Wiley Professional (1997).

Mahnken, R.; Stein, E.: A unified approach for parameter identification of inelastic material models in the frame of the finite element method. *Comput. Methods Appl. Mech. Engrg.*, 136, (1996), 225–258.

Mahnken, R.; Steinmann, P.: A finite element algorithm for parameter identification of material models for fluid saturated porous media. *Int. J. Numer. Anal. Meth. Geomech.*, 25, (2001), 415–434.

Marquardt, D.: An algorithm for least-squares estimation of nonlinear parameters. *SIAM J. Appl. Math.*, 11, (1963), 431–441.

Moritz, H.: General considerations regarding inverse and related problems. *Inverse Problems: Principles and Applications in Geophysics, Technology and Medicine*, 74, (1993), 11.

Nava, A.; Mazza, E.; Furrer, M.; Villiger, P.; Reinhart, W.: In vivo mechanical characterization of human liver. *Medical Image Analysis*, 12, (2008), 203–216.

Nocedal, J.; Wright, S. J.: *Numerical Optimization*. Springer-Verlag, New York (1999).

Pardis, N.; Talebanpour, B.; Ebrahimi, R.; Zomorodian, S.: Features of cyclic extrusion compression method, structure and materials properties. *Prod. Eng. Res. Devel.*, 4, (2010), 391–397.

Pardis, N.; Talebanpour, B.; Ebrahimi, R.; Zomorodian, S.: Features of cyclic extrusion compression method, structure and materials properties. *Materials Science and Engineering*, 528, (2011), 7537–7540.

Parhami, B.: *Computer Architecture: From Microprocessors To Supercomputers*. Oxford University Press (2005).

Piegl, L.; Tiller, W.: *The NURBS Book*. Springer Verlag Berlin, Heidelberg (1995).

Richert, M.: Features of cyclic extrusion compression method, structure and materials properties. *Solid State Phenomena*, 114, (2006), 19–28.

Schellenberg, D.; Kreißig, R.; Ihlemann, J.: Optimierungsstrategien im Bereich der Formoptimierung bei Massivumformverfahren. In: *Proceedings in Applied Mathematics and Mechanics (GAMM)*, page 543–544, Karlsruhe (2010).

Schellenberg, D.; Lindner, M.; Kreißig, R.: Nonlinear Optimization in Context with Parameter Identification and Shape Optimization. In: *Application Stochastics and Optimization Methodes*, Forming Technology Forum 07, pages 55–60, ETH Zürich (2007).

Schiavone, P.; Chassat, F.; Boudou, T.; Promayon, E.; Valdivia, F.; Payan, Y.: In vivo measurement of human brain elasticity using a light aspiration device. *Medical Image Analysis*, 13, (2009), 673–678.

Schneider, F.-J.: *Interpolation, Approximation und Konvertierung mit rationalen B-Splines*. Diss., RWTH Aachen (1993).

Schnur, D.; Zabaras, N. J.: An inverse method for determining elastic material properties and a material interface. *Int. J. Num. Eng.*, 33, (1992), 2039–2057.

Schumacher, A.: *Optimierung mechanischer Strukturen - Grundlagen und industrielle Anwendungen*. Springer Verlag Berlin, Heidelberg (2005).

Shutov, A.; Kreißig, R.: Regularized strategies for material parameter identification in the context of finite strain plasticity. *Technische Mechanik*, 30(1-3), (2010), 280–295.

Snir, M.: *MPI: The Complete Reference - Volume 1/2*. The MIT Press (1998).

Suh, J.-K.; Olberding, J.: A dual optimization method for the material parameter identification of a biphasic poroviscoelastic hydrogel: Potential application to hypercompliant soft tissues. *Journal of Biomechanics*, 39, (2006), 2468–2475.

Address: Dipl.-Inf. Hans Wulf, Dipl.-Ing. Dirk Schellenberg, Prof. Dr. Reiner Kreißig and Prof. Dr. Jörn Ihlemann, Department of Solid Mechanics, Chemnitz University of Technology, Chemnitz, Germany.
email: hans.wulf@mb.tu-chemnitz.de; dirk.schellenberg@mb.tu-chemnitz.de.; reiner.kreissig@mb.tu-chemnitz.de; joern.ihlemann@mb.tu-chemnitz.de